



HAL
open science

Experimental Study of O-2 Diffusion Coefficient Measurement at a Planar Gas-Liquid Interface by Planar Laser-Induced Fluorescence with Inhibition

Mélanie Jimenez, Nicolas Dietrich, Arnaud Cockx, Gilles Hébrard

► To cite this version:

Mélanie Jimenez, Nicolas Dietrich, Arnaud Cockx, Gilles Hébrard. Experimental Study of O-2 Diffusion Coefficient Measurement at a Planar Gas-Liquid Interface by Planar Laser-Induced Fluorescence with Inhibition. *AIChE Journal*, 2013, 59 (1), pp.325 - 333. 10.1002/aic.13805 . hal-01268214

HAL Id: hal-01268214

<https://hal.science/hal-01268214>

Submitted on 18 Jul 2021

HAL is a multi-disciplinary open access archive for the deposit and dissemination of scientific research documents, whether they are published or not. The documents may come from teaching and research institutions in France or abroad, or from public or private research centers.

L'archive ouverte pluridisciplinaire **HAL**, est destinée au dépôt et à la diffusion de documents scientifiques de niveau recherche, publiés ou non, émanant des établissements d'enseignement et de recherche français ou étrangers, des laboratoires publics ou privés.

Experimental study of O₂ diffusion coefficient measurement at a planar gas-liquid interface by PLIF with inhibition

JIMENEZ Mélanie^{a,b,c*}, DIETRICH Nicolas^{a,b,c}, COCKX Arnaud^{a,b,c}, HEBRARD Gilles^{a,b,c}

^a Université de Toulouse; INSA, UPS, INP; LISBP; F 31077 Toulouse, France

^b INRA, UMR792, Ingénierie des Systèmes Biologiques et des Procédés, F-31400 Toulouse, France

^c CNRS, UMR5504, F-31400 Toulouse, France

10

ABSTRACT

A new method for determining the molecular diffusivity of oxygen in liquids is presented in this paper. The technique was applied through a flat air-liquid interface in a Hele-Shaw cell (5×5×0.2 cm³) and was based on Planar Laser Induced Fluorescence (PLIF) with inhibition. A ruthenium complex (C₇₂H₄₈N₈O₆Ru) was used as the fluorescent dye sensitive to oxygen. A mathematical analysis was developed to determine the molecular diffusivity of oxygen simply by localizing the gas diffusion front. The specificity of this mathematical analysis is that it does not require the properties of the fluids
20 (such as the saturation concentration) to be considered, which is especially relevant for complex media that are sometimes difficult to characterize properly. This technique was applied to three different fluids (viscosities ranging from 1 to 2.4 mPa.s) corresponding to binary diffusion coefficients ranging from 9.5×10⁻¹⁰ to 2 ×10⁻⁹ m²/s. Experimental data were found with

* mjimenez@insa-toulouse.fr

an uncertainty of about 5% and were in good agreement with the literature. Particle Image Velocimetry and numerical simulations were also carried out to determine the optimal gas flow rate (0.01 L/s) to reach purely diffusive transfer, and the corresponding hydrodynamic profiles of the two phases.

30

40

1. Introduction

50 Gas-liquid mass transfer is of prime interest in several areas, from chemical engineering (bubble column, bioreactors) to environmental issues (waste water treatment, absorption of pollutants in oceans). Since it is a phenomenon related to the efficiency of the processes and to the pollution of natural resources, researches in this area have been many and varied. Nevertheless, some aspects of gas-liquid mass transfer remain unclear and would deserve some additional effort. For instance, a lack of knowledge persists in the molecular diffusivities of gases in liquids and thus in the mass transfer behavior in the vicinity of the gas-liquid interface.

Research in this domain has been intensive and several techniques have
60 been developed to measure experimental diffusion coefficients of gases in liquids: the diaphragm cell method (Hung and Dinius¹; Tham *et al.*²), the capillary cell method (Malik and Hayduk³), the polarographic diffusion cell method (Ho *et al.*⁴) and other techniques based on the use of microprobes (Hebrard *et al.*⁵; Jamnongwong *et al.*⁶), the laminar jet method (Sovova and Prochazka⁷), constant/decrease bubble size methods (Wise and Houghton⁸; de Blok and Fortuin⁹), to mention just a few. Optical techniques, such as interferometry, have also been largely developed to characterize diffusive process (Ambrosini *et al.*¹⁰). Due to their several well-known advantages (fast response, high resolution, non-invasive nature, reliability of the results *etc.*),
70 these techniques seem to be the most suitable ones for studying diffusive mechanisms. However, it has to be noted that they concern gas-gas or liquid-liquid systems in most cases (He *et al.*¹¹; Jamshidi-Ghaleh *et al.*¹²)

and rarely include the measurement of diffusion coefficients of gases in liquid media (Roetzel *et al.*¹³). As a consequence of the number of techniques available, a multitude of diffusivity measurements exist for a known gas-liquid system and their determination is thus still commonly restricted to the use of empirical correlations (*e.g.* Wilke and Chang¹⁴; Othmer and Thakar¹⁵) which are valid only under certain conditions (dilute solutions for instance).

80 Some authors have pointed out the importance and the difficulty of establishing accurate experiments for determining gas diffusion coefficients in liquids (Sovova and Prochazka⁷; Walker and Peirson¹⁶; Jamnongwong *et al.*⁶; Hebrard *et al.*⁵). On the whole, diffusive transfer observations are time-consuming and sensitive to any convective disruption, which complicates the experimental set up. Moreover, in turbulent media for instance, the thickness of the mass boundary layer can vary from ten to hundreds micrometers for slightly soluble gases (Herlina and Jirka¹⁷; Walker and Peirson¹⁶). High resolution systems are thus required for quantitative explorations in the vicinity of the interface and optical systems, such as
90 holographic interferometry, are widely used (Kutepov *et al.*¹⁸; Wylock *et al.*¹⁹).

The Planar Laser Induced Fluorescence (hereafter noted PLIF) is another optical system widely used for studying gas transfer in liquids. PLIF (Geddes²⁰) is based on the use of a fluorescent dye in the liquid medium, characterized by its sensitivity to specific parameters (gas concentrations, pH changes, *etc.*). Thanks to this sensitivity, gas absorption can be

visualized and concentration profiles can be derived with high spatial and temporal resolution. PLIF is thus a promising technique to shed light on gas-liquid transfer and many PLIF based studies have been carried out.

100 Wolff and Hanratty²¹ introduced PLIF with inhibition to visualize O₂ concentration near a gas-liquid interface. Many researchers (Wolff and Hanratty²²; Herlina and Jirka¹⁷; Variano and Cowen²³; Falkenroth *et al.*²⁴; Asher and Litchendorf²⁵; Francois *et al.*²⁶ among others) have continued to work on the same subject by studying the absorption of O₂ through flat, wavy or bubble interfaces. Similar experiments have been conducted with other gases such as CO₂ (Takehara and Etoh²⁷; Stöhr *et al.*²⁸) and HCl (Münsterer and Jähne²⁹). However, despite the various experiments carried out with PLIF on gas-liquid mass transfer, quantitative measurements have focused only on the determination of gas concentration profiles, liquid side
110 mass transfer coefficients or mass boundary layer thickness and have mainly concerned turbulent media. To the best of our knowledge, no diffusion coefficient measurements of gases in liquids, which require well-controlled and specific hydrodynamics, have been made using this technique.

The contribution of the work reported here is thus to set up a new and promising experiment, first to accurately visualize the pure diffusive process of oxygen through a planar air-liquid interface by PLIF with inhibition in a Hele-Shaw cell (5×5×0.2 cm³), then to measure oxygen concentration profile in the liquid phase near the interface and, finally, to determine the diffusion
120 coefficient of oxygen in the studied liquid using a simplified mathematical

solution. Experimental results are then compared to values from the literature. The particularity of this paper is also that it combines the PLIF technique with PIV (Particle Image Velocimetry) experiments and COMSOL simulations, first to determine the optimal gas flow rate allowing the diffusive process to take place and then to quantify the hydrodynamic fields in the two phases. The presented paper allows thus two fundamental aspects of gas-liquid transfer to be associated: diffusivity and hydrodynamic behavior.

130 *2. Determination of mass transfer equations in a Hele-Shaw cell*

Experiments based on a flat air-liquid interface were carried out in a Hele-Shaw cell (Hele Shaw³⁰). This cell's thickness (0.2 cm) is small compared to its height (5 cm) and width (5 cm), as depicted in Figure 1.

With such a configuration, it can be assumed that the problem is 2-dimensional (the contribution along the z axis can be neglected), and that a concentration gradient only appears along the x axis. The absence of convection in the x-direction is also assumed (see part 3 for further details on the experimental set-up and hypothesis validation).

140 Under these assumptions, mass transfer equations in the Hele-Shaw cell can be derived from Fick's law of diffusion (Fick³¹) as follows.

$$\frac{\partial C}{\partial t} = D \frac{\partial^2 C}{\partial x^2} \quad (1)$$

with C the gas concentration in the liquid phase (mg/L), D the molecular diffusivity of the gas in the liquid (m²/s), t the time (s) and x the distance to the gas-liquid interface (m).

The duration of the experiments being relatively short (~30 minutes) compared with the duration of the diffusive process of gas in liquid ($t \sim L^2/D = 833$ minutes for $L=1$ cm), the analytical solution in a semi-infinite medium is assumed (Crank³²).

$$\frac{C - C_0}{C_s - C_0} = 1 - \operatorname{erf}\left(\frac{x}{2\sqrt{Dt}}\right) \quad (2)$$

Where C_0 and C_s are the concentration in the bulk and at saturation respectively (mg/L) and $\operatorname{erf}(\cdot)$ is the function error defined as in (3) (Abramowitz and Stegun³³).

$$\operatorname{erf}(u) = \frac{2}{\sqrt{\pi}} \int_0^u \exp(-u^2) \cdot du \quad (3)$$

By setting up an experiment to measure $C(x,t)$ and assuming that C_0 and C_s are known, it is thus possible to determine D using (2).

However, the knowledge of the saturation concentration C_s is not as simple as wanted, especially in complex media (Slininger *et al.*³⁴; Ho *et al.*⁴; Schumpe³⁵). This paper thus proposes to determine the solution of (2) in

160 such a way that C_s can remain unknown.

Based on (2), the closed-form expression of $\frac{\partial^2 C}{\partial x^2}$ is given by (4).

$$\frac{\partial^2 C}{\partial x^2} = \frac{x}{\sqrt{\pi Dt} \cdot 2Dt} \cdot \exp\left(\frac{-x^2}{4Dt}\right) \cdot (C_s - C_0) \quad (4)$$

Now, let us introduce the gamma distribution as (5) (Upton and Cook³⁶)

$$f(X, k, \theta) = \frac{X^{k-1} \exp\left(\frac{-X}{\theta}\right)}{\Gamma(k) \cdot \theta^k} \quad (5)$$

Assuming that D is constant and with $X = x^2$ and $\theta = 4 \cdot D \cdot t$, it can be deduced that (6)

$$\frac{\partial^2 C}{\partial x^2} \propto \frac{X^{1/2}}{\theta^{3/2}} \exp\left(-\frac{X}{\theta}\right) \quad (6)$$

And thus that $k=3/2$ according to (5).

The relevance of the gamma distribution comes from the fact that its mode, *i.e.* the value of X maximizing $f(X, k, \theta)$, is defined by (7). (Upton and Cook³⁶)

$$X_{\max} = (k - 1) \cdot \theta, k \geq 1 \quad (7)$$

In the present study, the point where $\frac{\partial^2 C}{\partial x^2}$ is maximized at a given time represents the location of the maximum curvature of $C(x, t)$.

The diffusion front is thus characterized by (8).

$$X_{\max} = x_{\text{front}}^2 = \left(\frac{3}{2} - 1\right) \cdot 4Dt = 2Dt \quad (8)$$

However, the time, t , since the beginning of the diffusive process could be quite difficult to determine accurately, it is preferable to study the variation between two subsequent instants.

180

$$x_{\text{front } 1}^2 - x_{\text{front } 2}^2 = 2D(t_1 - t_2) \quad (9)$$

With x_{front} the distance between the gas-liquid interface and the x -position maximizing $\frac{\partial^2 C}{\partial x^2}$.

It is noteworthy that formulation (8) is similar to the Einstein and Smoluchowski equations of Brownian motion (Einstein³⁷; von

Smoluchowski³⁸) based on the kinetic molecular theory of gases (Islam³⁹). However, in our case, the determination of Equation (8) is directly based on the mathematical resolution of Fick's law and this equation is only valid at a specific and remarkable point, the point of maximum curvature $\frac{\partial^2 C}{\partial x^2}$ for a given time.

190 The relevance of this formulation has been mathematically proved and experimentally tested as shown in the results section.

Thus, according to (8) and (9), the method proposed here sets up an experimental technique able to accurately locate the diffusion front, thus the point x maximizing $\frac{\partial^2 C}{\partial x^2}$ and to determine the value of the diffusion coefficient D . Note that no additional properties of the gas or liquid media are required to estimate the molecular diffusion coefficient.

Based on (9), the uncertainty on the molecular diffusion coefficient determined is given by (10).

200

$$\Delta D = \frac{x_{front\ 1}^2 - x_{front\ 2}^2}{(t_1 - t_2)} \Delta x \quad (10)$$

Where ΔD and Δx are the uncertainty on the molecular diffusivity and on the x position respectively. From (10), it is straightforward to show that, the larger the time scale and the smaller the x uncertainty, the smaller the uncertainty on D . The technique proposed here for visualizing and locating the diffusion of O_2 in liquid is PLIF with inhibition.

3. Principle of PLIF with inhibition

Since details of this subject are available in the literature (Crimaldi⁴⁰; Geddes²⁰), only the basic principle of the technique is summarized in this section. PLIF, in a gas-liquid complex, is based on the use of a fluorescent dye that is incorporated in the liquid phase. This fluorescent dye is excited by a laser beam and re-emits light (fluorescence phenomenon) to return to its ground state. The light emitted by fluorescence is then recorded by a camera system. The fluorescent dye is chosen for its sensitivity to some parameters such as gas concentration, pH changes etc. In PLIF with inhibition, the fluorescent dye used is sensitive to the presence of oxygen in the liquid medium. Oxygen molecules inhibit the fluorescence process by colliding with molecules of the fluorescent dye; O₂ is called a “quencher” of fluorescence. In other words, when no oxygen is present in the liquid, the fluorescence is maximal, leading to a high light intensity recorded by the camera system. Conversely, when oxygen transfers in the liquid, the fluorescence is inhibited and thus darker areas appear (Figure 2).

Thanks to the inhibition of fluorescence, the concentration of O₂ can be determined from the intensity level recorded by the camera. The conversion into oxygen concentration is based on the Stern-Volmer equation (Stern and Volmer⁴¹).

$$\frac{I_Q}{I_0} = \frac{1}{1 + K_{sv}[Q]} \quad (11)$$

230 where K_{sv} is the Stern-Volmer constant (L/mg), $[Q]$ the quencher concentration (mg/L), and I_Q and I_0 the fluorescence intensities in presence and absence of quencher respectively. The intensity level recorded by the camera, characterized by grey levels, is inversely proportional to the concentration of O_2 in the liquid phase. The calibration curve can be determined by registering the fluorescence level of a solution with a known oxygen concentration, ranging from about 0 mg/l to the saturation concentration. These oxygen concentrations were measured by a specific probe (Mettler Toledo, $\pm 1\%$). Experimental points always fitted the Stern-Volmer equation with a square correlation coefficient higher than 99%

240 (Figure 3 $K_{sv} = 0.2$ L/mg).

4. Experimental set-up and procedure

4.1. Experimental set-up

The experimental set-up is presented in Figure 4. Each component is explained in detail in the following sections.

As explained in section 2, a Hele-Shaw [1] cell was used to reduce the problem to 2 dimensions. The Hele-Shaw cell was 5 cm high, 5 cm wide and
250 0.2 cm thick (Figure 1). The cell sides were transparent and made of PMMA (Polymethyl Methacrylate) with two gas orifices placed 1 cm below the top of the cell to allow the gas to flow [3]. An air flow [2][3] of about 0.01 L/s passed tangentially to the liquid interface without disrupting it. The control of the air flow was of prime importance to avoid disruption of the diffusion process by convection (See part 4.3).

In accordance with Dani *et al.*⁴² and Francois *et al.*²⁶, the liquid medium filling the Hele-Shaw cell consisted of the studied liquid, 25 mg/L of ruthenium complex (Nanomeps), $C_{72}H_{48}N_8O_6Ru$, to observe the fluorescence and 20% by mass of ethanol to solubilize the fluorescent dye. The
260 introduction of ethanol indubitably changed the properties of the liquid phase, however, this does not fundamentally distort the principle presented in this paper. The ruthenium complex was chosen for its excellent sensitivity to the presence of oxygen and thus its ability to improve the visualization of the O_2 diffusion. Experiments were performed for three different liquid media, whose properties are described in Table 1. Viscosity and density were measured with a Haake VT550 Viscotester (Thermo

scientific, Thermo Fisher Scientific Inc) and with a pycnometer (Brand Duran, $V = 25 \text{ cm}^3$) respectively.

270

The laser sheet [5] was produced by a Nd: Yag laser [4] (Quantel, $\lambda = 532 \text{ nm}$, 10 Hz, $200 \times 2 \text{ mJ}$) and controlled by a monitoring system [6]. The laser sheet crossed the Hele-Shaw cell vertically, along the xy plane. A Charge-Coupled-Device (CCD) camera [7] (Imager Intense, LaVision, 12 bits) was placed perpendicularly to the Nd: Yag laser, in front of the xy plane, to record the fluorescence level at the gas-liquid interface. A range of 2000 grey levels is available with this optical system. The size of the recorded pictures is $1040 \times 1376 \text{ pixels}^2$ which corresponds to a window of $\sim 9 \times 12 \text{ mm}^2$. A 105 mm objective (Micro-Nikkor 105 mm f/8, Nikon) and a 570 nm high-pass
280 filter added to the digital camera allowed the fluorescence of the ruthenium complex to be recorded while blocking the laser light. The Nd: Yag laser and the digital camera were synchronized by a synchronizer [8] (Programmable Trigger Unit, LaVision). Data were then collected using specific acquisition software (Davis 7.2, LaVision)[9].

Besides PLIF experiments, Particle Image Velocimetry was carried out to determine the velocity field in the liquid medium. Reflecting particles were added to the liquid medium and their motion was tracked with specific software. The experimental set-up was similar to the one described for PLIF except for the laser used (Dantec Dynamics Big Sky-Twins Nd: Yag laser, $\lambda =$
290 532 nm , 15 Hz, $30 \times 2 \text{ mJ}$). The software used to analyze the results was Flow Manager Version 4.60. The tracer particles used were silver-coated

hollow glass spheres, 20 μm in diameter, made by Dantec Dynamics. The size of the interrogation areas was 32×32 pixels². The delay between two successive images was 32 ms and an overlap of 50% was set.

4.2. *Experimental procedure*

The first step of the PLIF experiments consisted in determining the calibration curve to check the linearity of the laser and to obtain the conversion equation between grey level and oxygen concentration.

300 Then, after the preparation of the liquid medium composed of the studied liquid, ethanol and the ruthenium complex, the solution was deoxygenated by nitrogen [2] until the oxygen concentration almost reached zero (~ 0.45 mg/L). Meanwhile, and due to the small thickness of the Hele-Shaw cell, the optical system was precisely adjusted to generate a laser beam flashing between the vertical plates of the Hele-Shaw cell. The deoxygenated solution was then cautiously allowed into the Hele-Shaw cell. The liquid height was set to about 3 cm. A nitrogen flow ran above the interface to insure there was no oxygen intrusion into the liquid medium. After a few minutes, the gas was switched to air to insure an air flow of about 0.01 L/s. The gas
310 switch over corresponded to the time $t=0$. A laser sheet was generated every minute and five images were recorded simultaneously (10 Hz) each time. It corresponded to a duration of 0.5 s, which is completely negligible in comparison with the duration of the diffusive process. To avoid evaporation issues, the duration of the experiments was limited to about 30 minutes.

The gas-liquid interface was located for each time to check that no evaporation had occurred (See part 4.3).

The procedure for PIV experiments was similar that for PLIF experiments. However, an area sizing the Hele-Shaw cell dimensions was chosen to
320 visualize the whole velocity field in the liquid phase.

4.3. Precautions

To insure the accuracy of experiments, some aspects had to be considered with great care. As the Hele-Shaw cell had a small thickness, some capillarity issues were possible. It was of prime importance to limit the apparition of a meniscus because it could lead to a reflection during the laser flash, altering the results.

The insertion of the deoxygenated liquid was a critical step. It had to be carried out in such a way that the interface remained plane and the
330 pollution of the liquid phase by oxygen was limited. A picture was therefore recorded after the insertion of the liquid, while nitrogen flowed above the interface to insure that the interface was effectively flat and that the grey level corresponded to the lowest oxygen concentration determined by the calibration curve.

The gas switch from nitrogen to air had to be done slowly and the interface had to be kept plane without disrupting it. A poorly controlled flow could generate instabilities near the air-liquid interface as shown in Figure 5, where PLIF and PIV experiments are superimposed. Instabilities of this kind

can be assimilated to Rayleigh-Taylor finger instabilities (Rayleigh⁴³;
340 Taylor⁴⁴).

However, when a correct air flow was generated above the interface, no instabilities appeared and the diffusion process could continue. In this case, the velocity field near the air-liquid interface in the liquid phase corresponded to the one depicted in Figure 6.

In this figure, the hypothesis of absence of convection along the x-direction
350 is confirmed at the vicinity of the interface. The weak velocities are due to the configuration of the Hele-Shaw cell, whose walls slow down the liquid motion. It should be noted that, according to PIV experiments, the liquid runs in the side opposed to the gas inlet. In fact, due to the small size of the gas outlet, a loop was also generated in the gas phase. This phenomenon was confirmed by simulations depicted in Figure 7. These simulations were made with the COMSOL Multiphysics 3.5a software and are based on the 2D Space dimension with a laminar flow module and a stationary study type. On this figure, simulations are depicted in the gas phase and PIV results are superimposed to represent the liquid motion.

360

Experiments were carried out in a temperature regulated room at 20°C. However, the laser sheet flashing five times a minute on the Hele-Shaw cell could have created a temperature gradient, able to generate more convection than described previously. Tests with a thermal camera (FLIR Systems) were

conducted to check the temperature homogeneity in the Hele Shaw cell. The experimental set-up was the same as in the PLIF experiments except that the CCD camera ([7] in Figure 4) was replaced by the thermal camera. The thermal camera only recorded information from the external wall of the
370 Hele-Shaw cell. The temperature of this wall was measured for different numbers of laser flashes, each flash having a duration of a few nanoseconds. It revealed that the thermal gradient in the Hele-Shaw cell could reasonably be neglected as long as experiments required less than ten successive laser flashes. With five flashes each minute, our experimental set-up was thus assumed to avoid any thermal gradient and induced convection due to the laser sheet.

5. *Image processing*

Pictures registered during the experiments needed some image processing to give accurate quantitative results.

380

As explained in part 4, for each time, five images were recorded at 10 Hz. The first step of the image processing consisted of averaging each pixel over the five pictures to obtain a “mean” picture. This averaging can be considered as a denoising step although it engendered an uncertainty of 0.5 s on the time estimation.

The second step consisted of detecting the gas liquid interface. Due to reflection at the interface, a peak in the grey values was present in the vicinity of the interface as previously observed (Variano and Cowen²³;
390 Walker and Peirson¹⁶). As shown in Figure 8, the location of the peak was stable even after several minutes, so there was no evaporation or leakage in the cell. The peak appeared to be quite a Gaussian with a standard deviation corresponding to the interface position uncertainty. This uncertainty was about 13%.

Special precautions have been advised by Walker and Peirson¹⁶ in order to minimize the area lost by interface reflection. They managed to make oxygen concentration profile measurements within 28 μm of an air-water interface,
400 which is clearly better than the results presented here. However, their

experimental set-up required the camera to be inclined (8°). To focus the camera on the liquid interface and to determine the geometric calibration factor (conversion between pixel and mm), a ruler was inserted in the Hele-Shaw cell. When the ruler's graduations appeared clear on the recorded image, the focus had been correctly defined. However, an inclined camera also means an inclined ruler to obtain a clear image, which was not feasible in our 2-mm-thick Hele-Shaw cell. A thickness of 7 mm was required to correctly tilt the ruler.

410 Once the interface was located, the Beer Lambert attenuation due to the absorption of the laser light in the liquid phase had to be considered. This part of the image processing was the same as that described by Walker and Peirson¹⁶ and Falkenroth *et al.*²⁴. Since the fluorescent dye concentration was constant in the liquid media, absorption of the laser light depended only on the distance covered by the laser sheet. By modeling the Beer Lambert dispersion, the absorbance coefficient was determined and images were processed to correct this dispersion as shown in Figure 9.

The last step was the application of a Gaussian filter which averaged a
420 window of 5×5 pixels² to denoise the raw images.

6. Results

An example of visualization of the oxygen diffusion process in water (80% w/w) and ethanol (20% w/w) (Case 1) is shown in Figure 10.

At the beginning of the experiments ($t=0$), the solution had been fully deoxygenated, maximizing the fluorescence and thus the intensity recorded by the CCD. After some minutes, a plane darker area appeared on the recorded picture, indicating the diffusion of oxygen in the liquid. Times longer than 20 minutes have been considered in Figure 10 in order to visualize a sufficient oxygen gradient. Since some micrometers were corrupted in the x-direction due to the interface reflection, the maximum value of oxygen concentration measured near the interface reached almost 4 mg/L in spite of the expected saturation concentration at about 9 mg/L (Jamnongwong *et al.*⁶). Similar visualizations were obtained for the two other cases studied (Table 1) but the diffusion process was slower since the viscosity was higher than in Case 1.

Using pictures like those presented in Figure 10, it is possible to determine the oxygen concentration profile as a function of time, t , and distance to the interface, x . This was achieved by using the Stern-Volmer equation (11) and by averaging each line of the picture to obtain a mean value for each x position.

As explained in part 2.2, the determination of the oxygen molecular diffusivity requires the location of the diffusion front, and especially the x -

position maximizing $\frac{\partial^2 C}{\partial x^2}$ at a given time. To facilitate the determination of this maximum, experimental data were fitted to a 6th order polynomial, whose second derivative could be easily computed.

450 Values of $\frac{\partial^2 C}{\partial x^2}$ in the vicinity of the maximal position for study case 1 are shown in Figure 11.

Note that the location of the maximum, and thus of the front, obviously has to increase time after time since the diffusion process goes on. The distance between two successive maxima becomes smaller over time due to Fick's law (1). Since oxygen transfers in a fully deoxygenated solution, the exchange potential will become smaller and thus the diffusion process slower.

To determine the molecular diffusion coefficient, equation (9) was used with all the registered times that minimized the uncertainty on D (10). The
460 median value of D was considered as the molecular diffusivity in the liquid studied. Experimental values of D are presented in Table 2 and compared to values from the literature (Wilke and Chang¹⁴; Scheibel⁴⁵).

Good agreement was observed between experimental data and the commonly used correlations related to the determination of molecular diffusivity in aqueous media, confirming the accuracy of the method presented. A comparison among the three liquids studied clearly confirmed the relationship between viscosity and diffusivity. As shown in Figure 12, where slopes are directly proportional to the diffusion coefficients (slope =
470 2D), the higher the viscosity, the slower the diffusion process.

These experimental diffusion coefficients present small uncertainties since efforts have already been made to minimize them (10). The essential feature of this technique is that the diffusion coefficient measurement is accomplished in a short time (less than 30 minutes). The accuracy is high (less than 5%), and the amount of fluid necessary to achieve the measurement is small (~ 3 mL). Another important feature is that only the position and the time of a specific point are necessary for the measurement and no physical properties are required.

480

7. Conclusions

In this paper, a new and promising technique was presented to visualize the pure diffusive process of oxygen in an aqueous solution through a flat interface by PLIF with inhibition and to determine the diffusion coefficient of oxygen in liquids. The use of a Hele-Shaw cell allowed the problem to be restricted to a 2-dimensional analysis. Thanks to this simplification, the mathematical determination of the diffusion coefficient was simplified so that it only required the location of the diffusion front versus time. The proposed approach can also be generalized since other parameters, such as

490 the liquid properties, remain unknown, which is especially relevant in complex media. The PLIF technique with inhibition was relevant since it allowed, first, the pure diffusive process to be visualized and then the oxygen concentration profile to be accurately measured. This technique was validated in three different Newtonian fluids (viscosities ranging from 1 to

2.4 mPa.s) corresponding to binary diffusion coefficients ranging from 9.5×10^{-10} to 2×10^{-9} m²/s. However, improvements could be made so as to take the interface reflection into consideration. Particle Image Velocimetry and simulations determined the motion of the two phases and permitted to ensure that only a diffusive process occurred. The results concerning both
500 mass transfer and hydrodynamics were of prime interest since the analytical resolution was based on several hypotheses that needed to be validated. It was shown that, in such a configuration, no convection disrupted the diffusion process when the air flow was correctly chosen. Molecular diffusion coefficients were determined in different liquids to check the relevance of the technique. Good agreement was observed with the literature and uncertainty estimates were small (less than 5%) with this new technique. The viability of the PLIF technique for measuring diffusion coefficients of oxygen in liquids has been demonstrated in this paper. It could thus be generalized to other gases (such as CO₂) and other
510 transparent liquids to become a useful tool for diffusion coefficient measurement and visualization.

Acknowledgements

The financial assistance provided by the French Ministère de l'Éducation Nationale, de la Recherche et de la Technologie and Degremont is gratefully acknowledged. The federation Fermat is also thanked for its help. We are also grateful to Laurent Chatillon and coworkers for their technical support.

Nomenclature

C	Gas concentration	mg/L
D	Molecular diffusion coefficient	m ² /s
I	Fluorescence intensity	Grey level
k	Parameter of the gamma distribution	
K _{SV}	Stern-Volmer constant	L/mg
[O ₂]	Oxygen concentration	mg/L
[Q]	Quencher concentration	mg/L
t	Time	s
V	Volume	m ³
x	Distance to the interface	m
X	Parameter of the gamma distribution	
y	Tangentially position to x	m
<i>Greek letter</i>		m
Δx	Uncertainty on x position	m
ΔD	Uncertainty on D	m ² /s
ρ	Density	kg/m ³
μ	Viscosity	Pa.s
Γ	Gamma function	
θ	Parameter of the gamma distribution	
λ	Wavelength	nm

Subscripts

0	Gas concentration in the bulk region (C_0)	mg/L
	Fluorescence intensity in absence of quencher (I_0)	Grey level
s	Saturation concentration of the gas	mg/L
front	Location of the x maximizing the second derivative of C as a function of x	

520

Literature cited

1. Hung, G. W., & Dinius, R. H. (2011). Diffusivity of oxygen in electrolyte solutions. *J. Chem. Eng. Data*, 17(4), 449-451.
- 530 2. Tham, M. J., Bhatia, K. K., & Gubbins, K. F. (1967). Steady-state method for studying diffusion of gases in liquids. *Chemical Engineering Science*, 22(3), 309-311.
3. Malik, V. K., & Hayduk, W. (1968). A steady-state capillary cell method for measuring gas-liquid diffusion coefficients. *The Canadian Journal of Chemical Engineering*, 46(6), 462-466.
4. Ho, C. S., Ju, L.-K., Baddour, R. F., & Wang, D. I. C. (1988). Simultaneous measurement of oxygen diffusion coefficients and solubilities in electrolyte solutions with a polarographic oxygen electrode. *Chemical Engineering Science*, 43(11), 3093-3107.
- 540 5. Hebrard, G., Zeng, J., & Loubiere, K. (2009). Effect of surfactants on liquid side mass transfer coefficients: A new insight. *Chemical Engineering Journal*, 148(1), 132-138.
6. Jamnongwong, M., Loubiere, K., Dietrich, N., & Hébrard, G. (2010). Experimental study of oxygen diffusion coefficients in clean water containing salt, glucose or surfactant: Consequences on the liquid-side mass transfer coefficients. *Chemical Engineering Journal*, 165(3), 758-768.
- 550 7. Sovova, H., & Prochazka, J. (1976). A new method of measurement of diffusivities of gases in liquids. *Chemical Engineering Science*, 31(11), 1091-1097.
8. Wise, D. L., & Houghton, G. (1966). The diffusion coefficients of ten slightly soluble gases in water at 10–60°C. *Chemical Engineering Science*, 21(11), 999-1010.

- 560 9. de Blok, W. J., & Fortuin, J. M. H. (1981). Method for determining diffusion coefficients of slightly soluble gases in liquids. *Chemical Engineering Science*, 36(10), 1687-1694.
10. Ambrosini, D., Paoletti, D., & Rashidnia, N. (2008). Overview of diffusion measurements by optical techniques. *Optics and Lasers in Engineering*, 46(12), 852-864.
11. He, M., Guo, Y., Zhong, Q., & Zhang, Y. (2011). Determination of Binary Gas Diffusion Coefficients Using Digital Holographic Interferometry. *J. Chem. Eng. Data*, 55(9), 3318-3321.
- 570 12. K. Jamshidi-Ghaleh, M.T. Tavassoly and N. Mansour, Diffusion coefficient measurements of transparent liquid solutions using Moiré deflectometry. *J Phys D: Appl Phys*, 37 (2004), pp. 1993–1997.
13. Roetzel, W., Blömker, D., & Czarnetzki, W. (1997). Messung binärer Diffusionskoeffizienten von Gasen in Wasser mit Hilfe der holographischen Interferometrie. *Chemie Ingenieur Technik*, 69(5), 674-678.
- 580 14. Wilke, C. R., & Chang, P. (1955). Correlation of diffusion coefficients in dilute solutions. *AIChE Journal*, 1(2), 264-270.
15. Othmer, D. F., & Thakar, M. S. (1953). Correlating Diffusion Coefficient in Liquids. *Industrial & Engineering Chemistry*, 45(3), 589-593.
16. Walker, J., & Peirson, W. (2008). Measurement of gas transfer across wind-forced wavy air-water interfaces using laser-induced fluorescence. *Experiments in Fluids*, 44(2), 249-259.
- 590 17. Herlina, & Jirka, G. H. (2004). Application of LIF to investigate gas transfer near the air-water interface in a grid-stirred tank. *Experiments in Fluids*, 37(3), 341-349.
18. Kutepov A. M, Pokusaev B. G, Kazenin D. A, Karlov S. P, & Vyazmin A. V. (s. d.). Interfacial Mass Transfer in the Liquid-Gas System: An Optical Study.
19. Wylock, C., Dehaeck, S., Cartage, T., Colinet, P., & Haut, B. (2011). Experimental study of gas-liquid mass transfer coupled with chemical reactions by digital holographic interferometry. *Chemical Engineering Science*, In Press, Corrected Proof.
- 600 20. Geddes, C. D. (2001). Optical halide sensing using fluorescence quenching: theory, simulations and applications - a review. *Measurement Science and Technology*, 12(9), R53-R88.
21. Wolff LM, Liu ZC, Hanratty TJ (1990) A fluorescence technique to measure concentration gradients near an interface. Proc 2nd Int Symp on Gas Transfer at Water Surfaces, pp 210-218.

610

22. Wolff, L. M., & Hanratty, T. J. (1994). Instantaneous concentration profiles of oxygen accompanying absorption in a stratified flow. *Experiments in Fluids*, 16(6), 385-392.

23. Variano, E. A., & Cowen, E. A. (2007). Quantitative Imaging of CO₂ Transfer at an Unsheared Free Surface. *Transport at the Air-Sea Interface*, Environmental Science and Engineering (p. 43-57). Springer Berlin Heidelberg.

620

24. Falkenroth, A., Degreif, K., & Jähne, Bernd. (2007). Visualisation of Oxygen Concentration Fields in the Mass Boundary Layer by Fluorescence Quenching. *Transport at the Air-Sea Interface*, Environmental Science and Engineering (p. 59-72). Springer Berlin Heidelberg.

25. Asher, W. E., & Litchendorf, T. M. (2008). Visualizing near-surface concentration fluctuations using laser-induced fluorescence. *Experiments in Fluids*, 46(2), 243-253.

630

26. Francois, J., Dietrich, N., Guiraud, P., & Cockx, A. (2011). Direct measurement of mass transfer around a single bubble by micro-PLIFI. *Chemical Engineering Science*, In Press, Accepted Manuscript.

27. Takehara K, Etoh GT (2002) A direct visualization method of CO₂ gas transfer at water surface driven by wind waves. In: Donelan M, Drennan WM, Saltzman ES, Wanninkhof R (eds) Gas transfer at water surfaces. American Geophysical Union, Washington, DC, pp 89-95.

640

28. Stöhr, M., Schanze, J., & Khalili, A. (2009). Visualization of gas-liquid mass transfer and wake structure of rising bubbles using pH-sensitive PLIF. *Experiments in Fluids*, 47(1), 135-143.

29. Münsterer, T., & Jähne, B. (1998). LIF measurements of concentration profiles in the aqueous mass boundary layer. *Experiments in Fluids*, 25(3), 190-196.

30. Hele-Shaw, H.S. 1898, The flow of water, *Nature*, v. 58, p. 34-36.

31. Fick, A. (1855). Ueber Diffusion. *Annalen der Physik*, 170(1), 59-86.

650

32. Crank, J. (John). (1975). *The mathematics of diffusion / by J. Crank*. Oxford science publications. Oxford [England]: Clarendon Press.

33. Abramowitz, M., & Stegun, I. A. (1964). *Handbook of mathematical functions with formulas, graphs, and mathematical tables*. Courier Dover Publications.

34. Slininger, P. J., Petroski, R. J., Bothast, R. J., Ladisch, M. R., & Okos, M. R. (1989). Measurement of oxygen solubility in fermentation media: A colorimetric method. *Biotechnology and Bioengineering*, 33(5), 578-583.

660

35. Schumpe et al., 1982 A. Schumpe, G. Quicker and W.-D. Deckwer, Gas solubilities in microbial culture media. *Adv. Biochem. Engng*, 24 (1982), pp. 1–38.

36. Upton, G. J. G., & Cook, I. (2008). *A dictionary of statistics*. Oxford University Press.

37. Einstein, A. (2005). Zur Theorie der Brownschen Bewegung [AdP 19, 371 (1906)]. *Annalen der Physik*, 14(S1), 248-258.

670

38. von Smoluchowski, M. (1906). Zur kinetischen Theorie der Brownschen Molekularbewegung und der Suspensionen. *Annalen der Physik*, 326(14), 756-780.

39. Islam, M. A. (2004). Einstein–Smoluchowski Diffusion Equation: A Discussion. *Physica Scripta*, 70(2-3), 120-125.

40. Crimaldi, J. (2008). Planar laser induced fluorescence in aqueous flows. *Experiments in Fluids*, 44(6), 851-863.

680

41. Stern, O. & Volmer, M. (1919) On the quenching time of fluorescence. *Physik Z.* 20, 183–188.

42. Dani, A., Guiraud, P., Cockx, A., 2007. Local measurement of oxygen transfer around a single bubble by planar laser-induced fluorescence. *Chemical Engineering Science* 62, 7245–7252.

43. Rayleigh. (1882). Investigation of the Character of the Equilibrium of an Incompressible Heavy Fluid of Variable Density. *Proceedings of the London Mathematical Society*, s1-14(1), 170 -177.

690

44. Taylor, G. (1950). The Instability of Liquid Surfaces when Accelerated in a Direction Perpendicular to their Planes. I. *Proceedings of the Royal Society of London. Series A, Mathematical and Physical Sciences*, 201(1065), 192-196.

45. Scheibel, E. G. (2011). Physical Chemistry in Chemical Engineering Design. *Ind. Eng. Chem.*, 46(8), 1569-1579.

700

Experimental study of O₂ diffusion coefficient measurement at a planar gas-liquid interface by PLIF with inhibition

JIMENEZ Mélanie^{a,b,c*}, DIETRICH Nicolas^{a,b,c}, COCKX Arnaud^{a,b,c}, HEBRARD Gilles^{a,b,c}

^a Université de Toulouse; INSA, UPS, INP; LISBP; F 31077 Toulouse, France

^b INRA, UMR792, Ingénierie des Systèmes Biologiques et des Procédés, F-31400 Toulouse, France

^c CNRS, UMR5504, F-31400 Toulouse, France

10

Figures content

- Figure 1* *Hele-Shaw cell*
- Figure 2* *Fluorescence quenching by oxygen in the liquid phase*
- Figure 3* *Calibration curve according to the Stern-Volmer equation*
- Figure 4* *Experimental set-up for PLIF experiments*
- Figure 5* *Instabilities at the air-liquid interface due to too high gas flow rates*
- Figure 6* *Velocity field in the liquid phase near the interface (Case 1) by PIV*
- Figure 7* *Velocity field (Case 1) in the liquid phase by PIV and in gas phase by COMSOL simulations in the Hele-Shaw cell*
- Figure 8* *Reflection at the gas-liquid interface*
- Figure 9* *Correction of the Beer Lambert attenuation*
- Figure 10* *Evolution of oxygen diffusion in the liquid*
- Figure 11* *Evolution of the second derivative of C with respect to x*
- Figure 12* *Evolution of x^2_{front} as a function of time for the three cases studied*

* mjimenez@insa-toulouse.fr

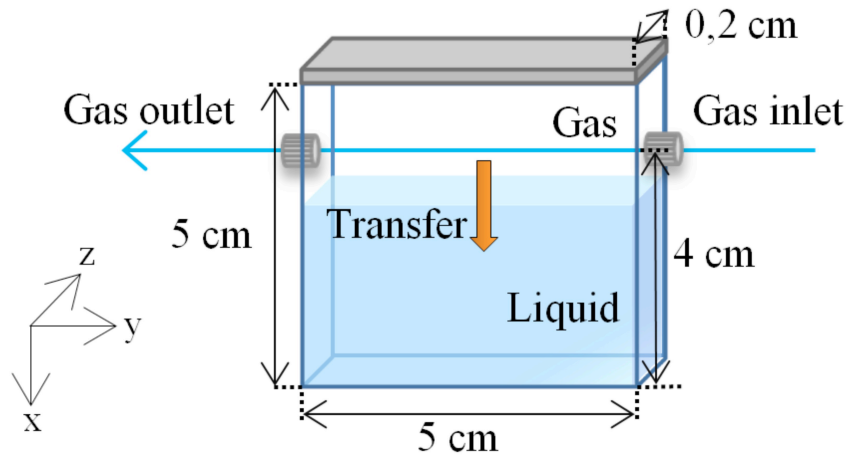
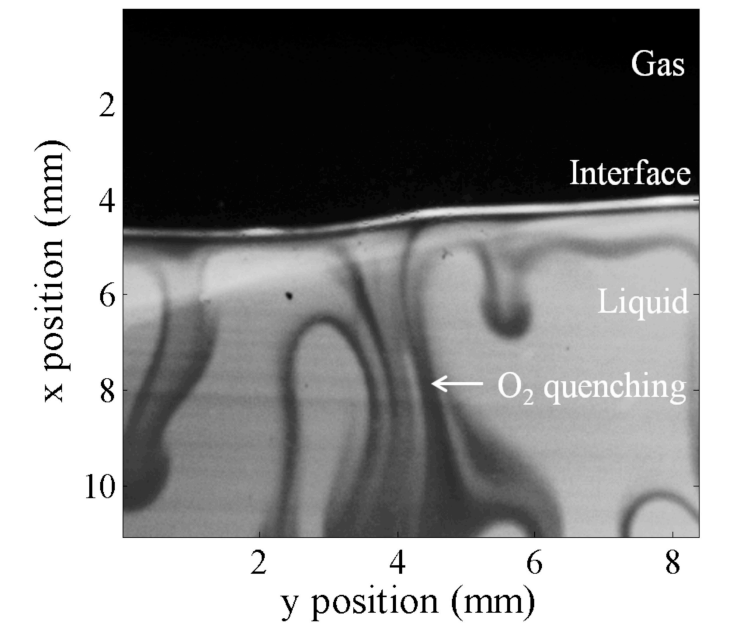


Figure 1. Hele-Shaw cell



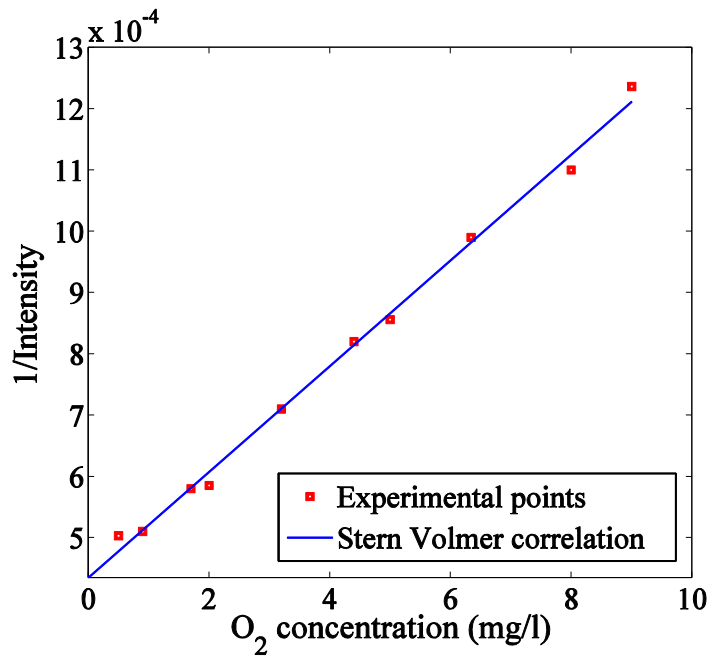


Figure 3. Calibration curve according to the Stern-Volmer equation

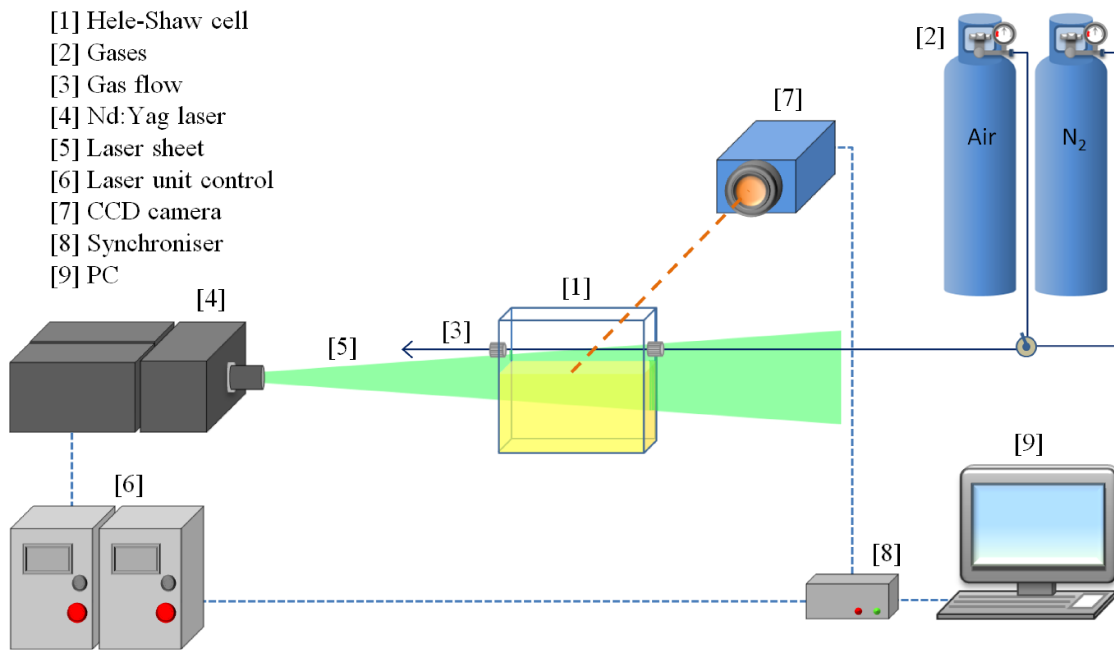


Figure 4. Experimental set-up for PLIF experiments

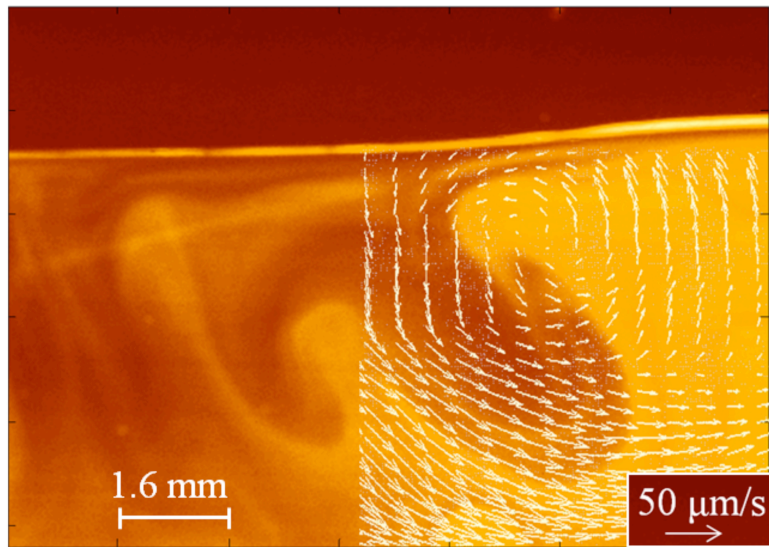


Figure 5. Instabilities at the air-liquid interface due to too-high gas flow rates

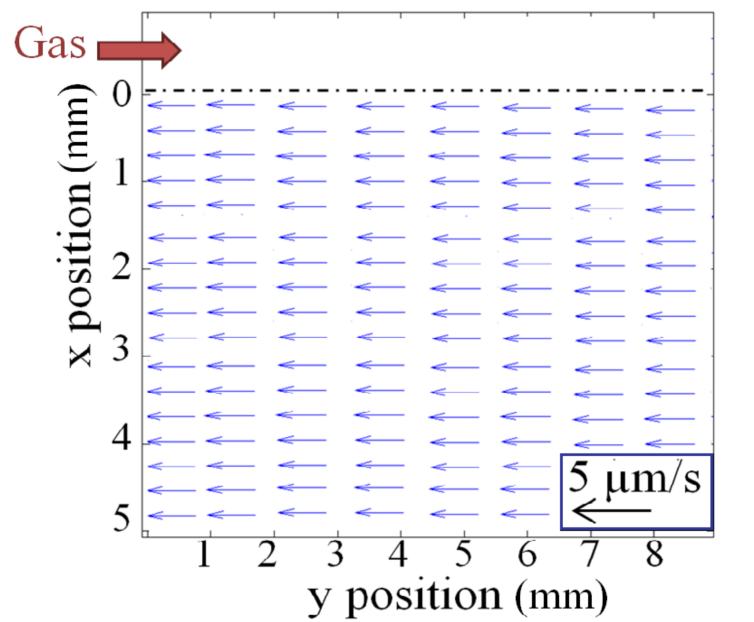


Figure 6. Velocity field in the liquid phase near the interface (Case 1) by PIV

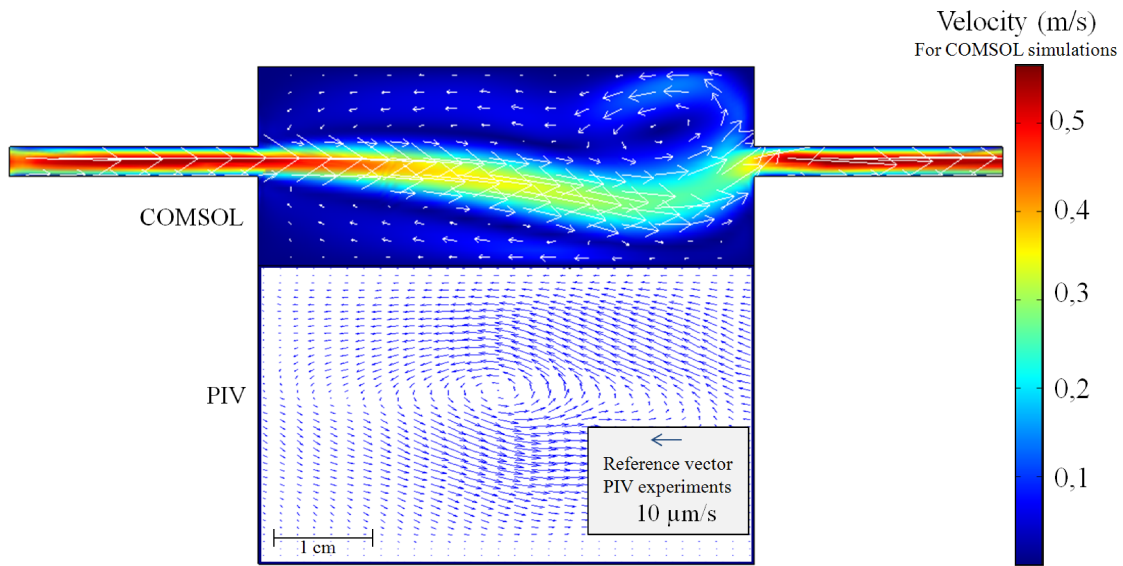


Figure 7. Velocity field (Case 1) in the liquid phase by PIV and in the gas phase by COMSOL simulations in the Hele-Shaw cell

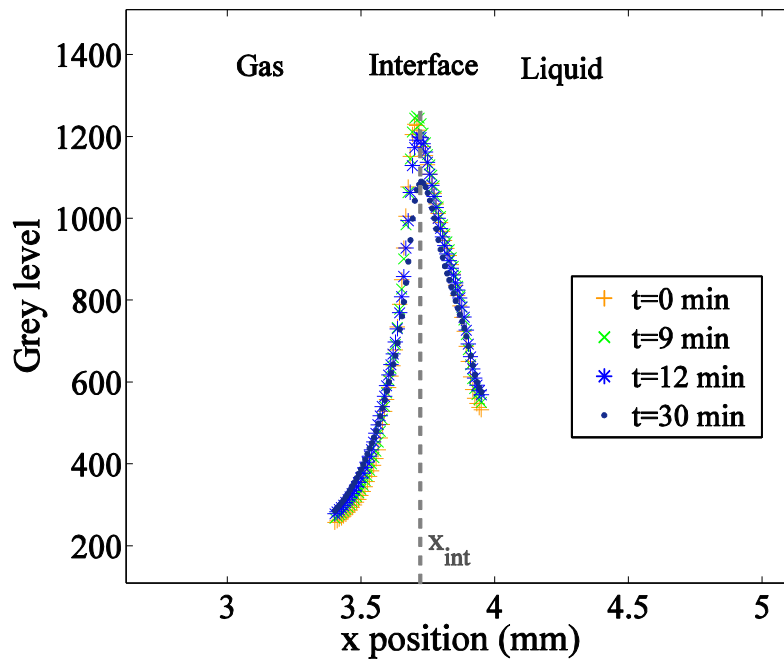


Figure 8. Reflection at the gas-liquid interface

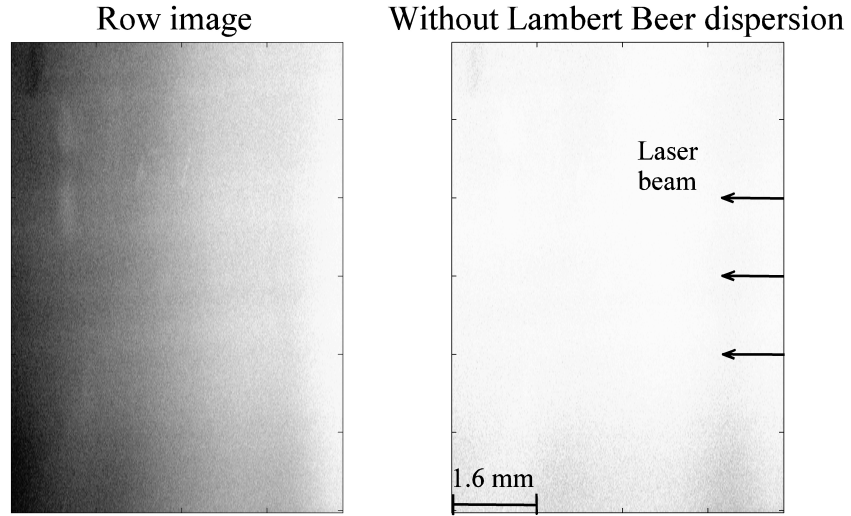


Figure 9. Correction of the Beer Lambert attenuation

50

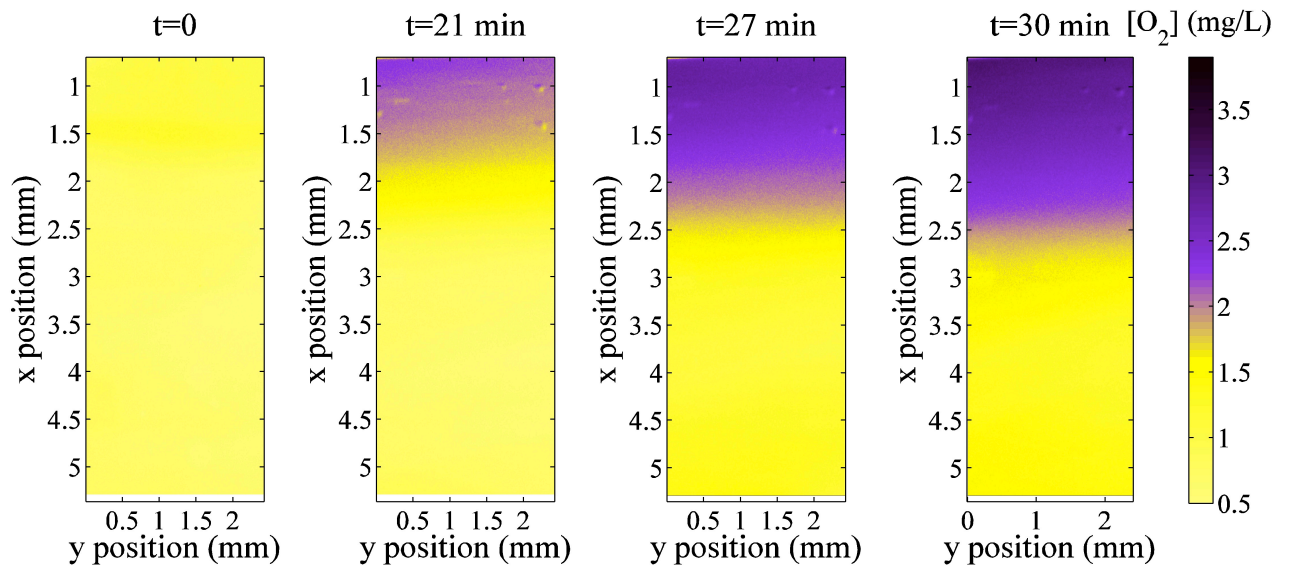


Figure 10. Evolution of oxygen diffusion in the liquid

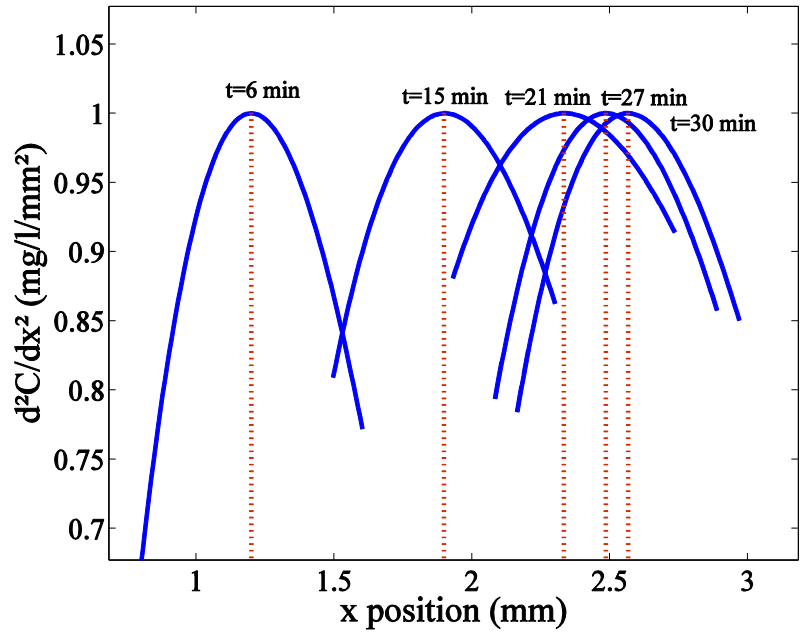


Figure 11. Evolution of the second derivative of C with respect to x

60

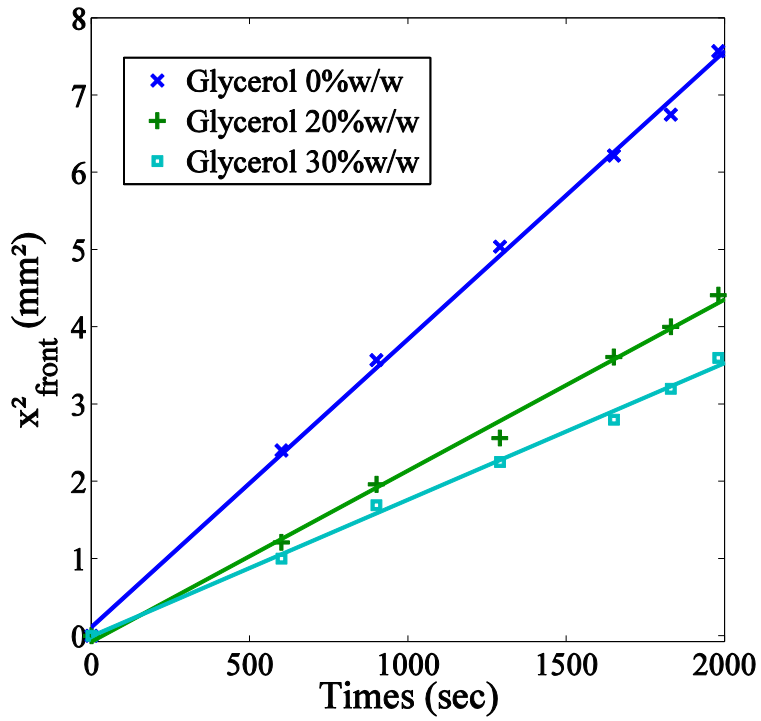


Figure 12. Evolution of x^2_{front} as a function of time for the three cases studied

Experimental study of O₂ diffusion coefficient measurement at a planar gas-liquid interface by PLIF with inhibition

JIMENEZ Mélanie^{a,b,c*}, DIETRICH Nicolas^{a,b,c}, COCKX Arnaud^{a,b,c}, HEBRARD Gilles^{a,b,c}

^a Université de Toulouse; INSA, UPS, INP; LISBP; F 31077 Toulouse, France

^b INRA, UMR792, Ingénierie des Systèmes Biologiques et des Procédés, F-31400 Toulouse, France

^c CNRS, UMR5504, F-31400 Toulouse, France

10

Table content

Table 1 *Characteristics of the liquid media studied*

Table 2 *Experimental results compared to correlations in the literature*

20

30

* mjimenez@insa-toulouse.fr

Case	Water (%w/w)	Ethanol (%w/w)	Glycerol (%w/w)	ρ (kg/m ³)	μ (Pa.s)
1	80	20	0	970	0.0010
2	60	20	20	1029	0.0017
3	50	20	30	1042	0.0024

Table 1. Characteristics of the liquid media studied

40

Case	D_{exp} (m ² /s)	$\Delta D/D$	Wilke and Chang ¹⁴	Scheibel ⁴⁵
1	1.9×10^{-9}	3%	1.994×10^{-9}	2.02×10^{-9}
2	1.2×10^{-9}	3%	1.3×10^{-9}	1.19×10^{-9}
3	9.47×10^{-10}	5%	9.5×10^{-10}	8.4×10^{-10}

Table 2. Experimental results compared to correlations in the literature